NAPRT Expression and Epigenetic Regulation in Pediatric Rhabdomyosarcoma as a Potential Biomarker for NAMPT Inhibition

Angela Kim[1,2,3], Prateek Bhardwaj[2], Shahyan Rehman[4], Sophia J. Zhao[3], Karlie N. Lucas[2], Katelyn J. Noronha[5], Deepti Bhatt[3], Sam Friedman[6], Raffaella Morotti[7], Ranjini K. Sundaram[2], Filemon S. Dela Cruz[8], Tamar Y. Feinberg[8], Subhash Ramakrishnan[9], Wei Xue[10], Donald A. Barkauskas[11], David Hall[9], Jack F. Shern[12], Wenyue Sun[13], Frederic G. Barr[13], Jae-Sung Yi[14], Josh Spurrier[14], Amy Yu[12], Charles Brenner[15], Collin D. Heer[2], Christine M. Heske[12], and Juan C. Vasquez[3,16]

ABSTRACT

New treatments are needed to improve survival in children with rhabdomyosarcoma (RMS). Nicotinamide adenine dinucleotide (NAD^+) biosynthesis, regulated by the enzymes nicotinic acid phosphoribosyltransferase (NAPRT) and nicotinamide phosphoribosyltransferase (NAMPT), represents a metabolic vulnerability due to high NAD^+ turnover in cancers. Although NAMPT inhibitors (NAMPTi) show preclinical promise, clinical translation has been limited by toxicity and the lack of predictive biomarkers. In this study, we evaluated NAPRT expression in RMS and its potential as an actionable biomarker to guide NAMPTi therapy. *NAPRT* promoter methylation, transcript levels, and protein expression were assessed in RMS cells, patient-derived xenografts (PDX), and primary tumors ($n = 109$) from the Children's Oncology Group. *In vitro* sensitivity to NAMPTi was tested in isogenic RMS cell lines, examining the role of NAPRT expression in mediating cytotoxicity and the ability of nicotinic acid (NA) to rescue viability. *In vivo* efficacy was assessed using cell-derived, NAPRT-isogenic, and orthotopic PDX models. *NAPRT* promoter hypermethylation was found in a subset of RMS models and patient samples. Immunohistochemistry showed loss of NAPRT protein in 30% to 40% of tumors, defined as <1% tumor cell staining. Methylation modestly correlated with protein expression. NAPRT-deficient cells were highly sensitive to NAMPTi, driven by NAD^+ depletion and not reversible with NA. *In vivo*, NAMPTi induced significant tumor regression, which was not abrogated with NA administration in NAPRT-deficient models. NAPRT loss occurs in a subset of RMS and may offer a biomarker-driven strategy to expand the therapeutic window of NAMPTi. Further research is needed to understand *NAPRT* regulation and optimize biomarker assays in future clinical trials.

Introduction

Rhabdomyosarcoma (RMS) is the most common soft tissue sarcoma among children, accounting for 5% of all pediatric cancers (1). The current treatment strategy for RMS consists of chemotherapy, surgical resection, and/or radiotherapy. Although outcomes for patients with low-risk RMS are excellent, the long-term survival rates for patients with metastatic or high-risk disease are less than 30% (2). As there have been no significant improvements in the overall survival for pediatric patients with high-risk RMS over the last several decades, there is a dire need to develop new treatments (3, 4).

Nicotinamide adenine dinucleotide (NAD^+) plays a vital role in cellular energy metabolism as an essential coenzyme for glycolysis, the tricarboxylic acid (TCA) cycle, oxidative phosphorylation, fatty acid metabolism, antioxidant metabolism, and serine biosynthesis, all of which contribute to cancer progression (5–7). Furthermore, cancer cells exhibit several characteristic features that drive their reliance on NAD^+ production, including dysregulated metabolism, rapid proliferation, and continuous NAD^+ consumption by NAD^+-degrading enzymes, such as PARPs and sirtuins (8, 9).

Given this dependency, numerous studies have suggested that disrupting NAD^+ biosynthesis could serve as a potential therapeutic anticancer strategy (10). Normal cells synthesize NAD^+ primarily through the Preiss–Handler and Salvage pathways and are rate-limited by nicotinic acid phosphoribosyltransferase (NAPRT) and

[1]Department of Pathology and Molecular Medicine, Yale School of Medicine, New Haven, Connecticut. [2]Department of Therapeutic Radiology, Yale School of Medicine, New Haven, Connecticut. [3]Department of Pediatrics, Yale School of Medicine, New Haven, Connecticut. [4]Department of Surgery, Yale School of Medicine, New Haven, Connecticut. [5]Department of Molecular Biophysics and Biochemistry, Yale School of Medicine, New Haven, Connecticut. [6]Yale Center for Research Computing, Yale University, New Haven, Connecticut. [7]Department of Pathology, Yale School of Medicine, New Haven, Connecticut. [8]Department of Pediatrics, Memorial Sloan Kettering Cancer Center, New York, New York. [9]Children's Oncology Group, Monrovia, California. [10]Department of Biostatistics, University of Florida, Gainesville, Florida. [11]Department of Preventive Medicine, Keck School of Medicine, University of Southern California, Los Angeles, California. [12]Pediatric Oncology Branch, Center for Cancer Research, National Cancer Institute, National Institutes of Health, Bethesda, Maryland. [13]Laboratory of Pathology, Center for Cancer Research, National Cancer Institute, National Institutes of Health, Bethesda, Maryland. [14]Alphina Therapeutics, New Haven, Connecticut. [15]Department of Diabetes and Cancer Metabolism, City of Hope, Duarte, California. [16]Program in Translation Biomedicine, Yale Graduate School of Arts and Sciences, New Haven, Connecticut.

A. Kim and P. Bhardwaj contributed equally to this article.

Corresponding Author: Juan C. Vasquez, Pediatric Hematology/Oncology, Yale University, 15 York Street, LMP 2073, New Haven, CT 06510. E-mail: Juan.Vasquez@yale.edu

Mol Cancer Ther 2026;XX:XX–XX

doi: 10.1158/1535-7163.MCT-25-0619

nicotinamide phosphoribosyltransferase (NAMPT), respectively (**Fig. 1A**; ref. 10). Preclinical studies have demonstrated that pharmacologic NAMPT inhibition effectively depletes NAD^+, leading to cytotoxicity in cancer cells (11–14). However, early-phase clinical trials of NAMPT inhibitors (NAMPTi) in unselected adult patients with advanced cancers showed few objective responses and were limited by dose-limiting toxicities, including bone marrow suppression, particularly thrombocytopenia (15–17). Although retinal and cardiac toxicities were noted in preclinical animal studies, these were not reported in humans (18–20).

NAMPTi have not been clinically tested in pediatric solid tumors. Notably, there is emerging evidence that pediatric bone and soft-tissue sarcomas show exquisite sensitivity to NAMPTi, potentially due to unique metabolic vulnerabilities and intrinsic defects in DNA damage repair that are exacerbated by inhibition of NAD^+-dependent DNA repair enzymes (9, 21–28). However, the lack of a known actionable biomarker still limits clinical translation. Most normal tissues express *NAPRT*, whereas a significant proportion of tumor tissues do not (13, 29). Previous work from our group and others indicates that loss of *NAPRT* expression by tumor-specific promoter CpG island methylation may provide a novel biomarker for sensitivity to NAMPTi (9, 13, 26, 28–31).

In this study, we found that a subset of tumors across multiple RMS subtypes, including both FOXO1 fusion–positive and fusion–negative, harbor *NAPRT* promoter methylation and loss of NAPRT protein expression. Moreover, NAPRT-deficient RMS models were highly sensitive to NAMPTi *in vitro*, and cytotoxicity was not rescued by nicotinic acid (NA) supplementation, suggesting that the Preiss–Handler pathway is not functional in these cells (**Fig. 1A**). *In vivo*, NAMPTi resulted in significant tumor regression in NAPRT-deficient RMS orthotopic models, which was not reversed by NA administration, whereas NA completely abrogated NAMPTi efficacy in NAPRT-expressing tumors. These observations were mechanistically confirmed by the rescue of NAD^+ pools only in

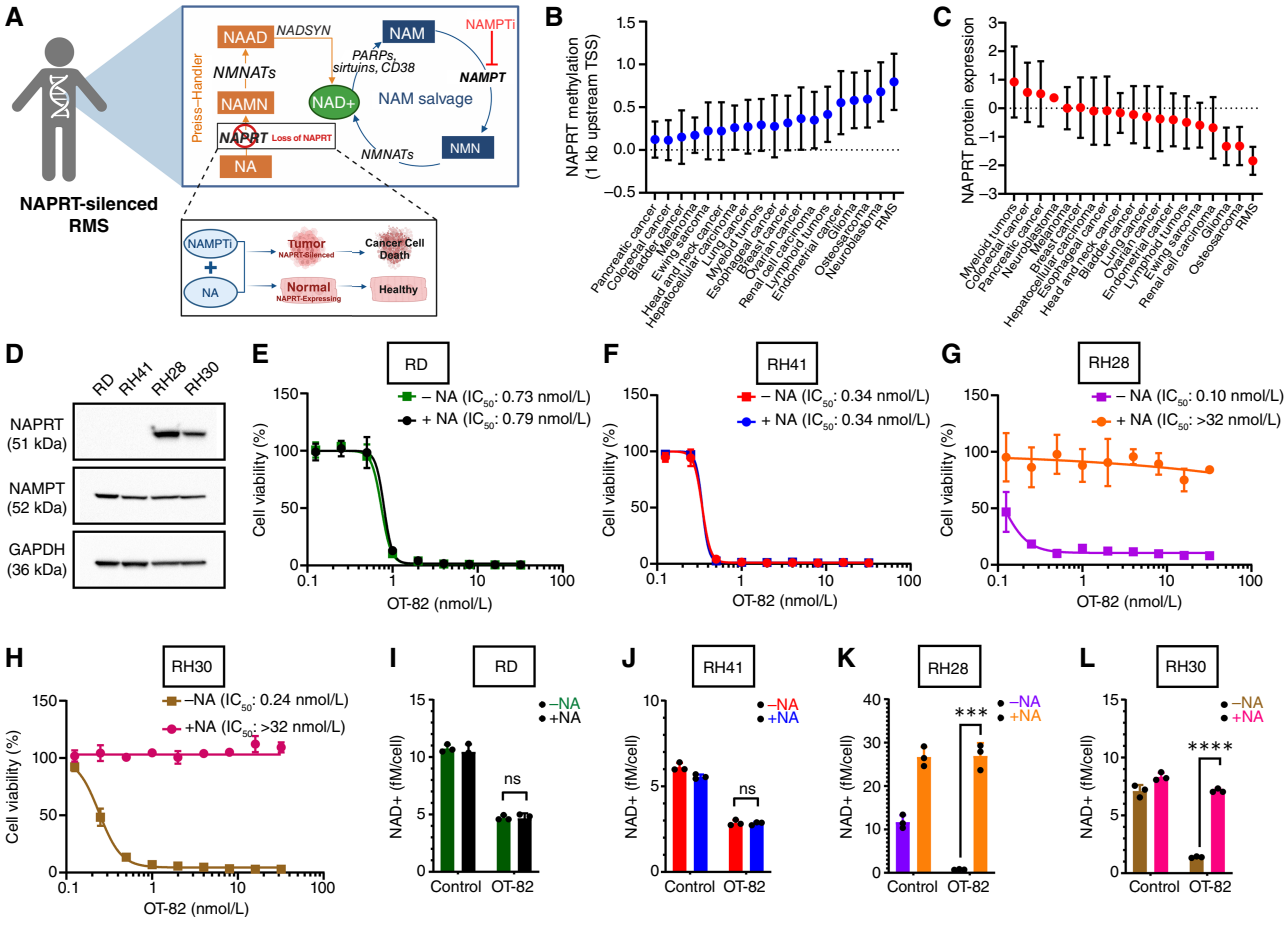

Figure 1.

RMS models display loss of NAPRT and sensitivity to OT-82 that is not rescued through the Preiss–Handler pathway. **A,** Schematic of NAD^+ biosynthesis pathways and the "protective rescue" paradigm in tumors with loss of NAPRT. **B,** Plot illustrating the methylation of *NAPRT* across various cancer types. *NAPRT* is hypermethylated in RMS. **C,** Plot illustrating NAPRT protein expression across various cancer types. Loss of NAPRT protein expression is observed in RMS. **D,** Protein expression of NAPRT in four RMS models by Western blot. **E** and **F,** Cell viability in NAPRT-deficient RD (**E**) and RH41 (**F**) cells treated with increasing concentrations of OT-82 for 6 days with or without 10 μmol/L NA. **G** and **H,** Cell viability in NAPRT-expressing RH28 (**G**) and RH30 (**H**) treated with increasing concentrations of OT-82 for 6 days with or without 10 μmol/L NA. **I–L,** Total NAD^+ quantification after 24 hours in RD (**I**), RH41 (**J**), RH28 (**K**), and RH30 (**L**) treated with respective IC_{50} concentrations of OT-82 with or without 10 μmol/L NA. The data are plotted as means with error bars indicating SEM. ***, $P < 0.001$; ****, $P < 0.0001$; n.s., not significant. GAPDH, glyceraldehyde-3-phosphate dehydrogenase.

NAPRT-expressing models upon NA supplementation. Overall, these data suggest that NAPRT loss may serve as a predictive biomarker in RMS tumors by inducing a synthetic lethal interaction with NAD^+-depleting agents and providing an opportunity to widen the therapeutic index with NA supplementation.

Materials and Methods

Cell culture

RD cells were cultured in Dulbecco's Modified Eagle Medium (Gibco). RH28, RH30, and RH41 cells were cultured in Roswell Park Memorial Institute (Gibco). All media formulations contained 10% fetal bovine serum (Sigma) and 1% penicillin–streptomycin (Gibco). *Mycoplasma* testing was performed routinely using the MycoAlert assay kit (Lonza Biosciences). All cell cultures were maintained and treated in 5% CO_2, 20% O_2, and humidified in a 37°C incubator unless otherwise noted. Cells were collected for experiments within P3 to P10 to ensure experimental reproducibility and cell health. Cell lines were authenticated through the Yale Keck Biotechnology Core with short tandem repeat (STR) genotyping by fragment analysis. STR profiles generated via the Yale Keck Core will be made available upon request. RD (CCL-136; PRID: CVCL_1649) cells were obtained from ATCC. RH41 (PRID: CVCL_2176) and RH30 (PRID: CVCL_0041) cells were obtained from the Children's Oncology Group (COG) repository. RH28 (PRID: CVCL_8752) cells were a gift from Dr. Corinne Linardic's laboratory.

Isogenic model generation

RH41 cells were transfected with 2 μg of *NAPRT* cDNA plasmid (GenScript, cat. #OHu28558D) using Lipofectamine 3000 (Thermo Fisher Scientific). Forty-eight hours after transfection, cells were treated with G418 (Geneticin) to select for NAPRT-expressing cells. When cells were ~80% confluent, a flow-sorted single-cell generation was performed in 96-well plates. NAPRT overexpression was confirmed through immunoblotting and functionally validated through a cell proliferation assay.

RH30 cells were transfected with 37.5 pmol/L of respective sgRNA [CRISPR948669_SGM (gRNA1); CRISPR948672_SGM (gRNA2)] and 6.25 μg of Cas9 enzyme using Lipofectamine CRISPRMAX (Thermo Fisher Scientific). When cells were 70% to 80% confluent, approximately 48 hours after transfection, single-cell clones were isolated using limited dilution cloning in 96-well plates. NAPRT loss was validated by immunoblotting and a functional cell-based assay.

Rhabdosphere generation

NAPRT-deficient RH41 cells were cultured in neurobasal medium (Gibco) supplemented with 1× B-27 (Gibco), 80 ng/mL bFGF (STEMCELL Technologies), and 40 ng/mL EGF (STEMCELL Technologies; refs. 32, 33). Rhabdospheres were supplemented with nutrient-proficient neurobasal medium as mentioned above every 48 hours. Spheres were passaged once the media became acidic, approximately every 48 to 72 hours. After P5, cell viability assays with CellTiter-Glo (Promega) were performed on the rhabdospheres. The generation of rhabdospheres was verified through SOX2 expression (BD Biosciences, Clone O30-678; cat. #562139; PRID: AB_10897844) via flow cytometry (Beckman Coulter Cytoflex LX).

In vitro chemical treatments

FK866 (Selleck Chemicals) and OT-82 (Selleck Chemicals) were dissolved in DMSO and used for treatment as indicated (34, 35). FK866 and OT-82 were aliquoted and stored at −80°C. NA (Sigma-Aldrich) was solubilized in 1 mol/L NaOH and then diluted in complete media immediately prior to treatment, either alone or in combination with FK866 or OT-82, as indicated. Nicotinamide mononucleotide (NMN; Sigma-Aldrich) was diluted in PBS prior to treatment. Nicotinamide riboside (NR; Selleck Chemicals) was diluted in DMSO prior to treatment. NA, NMN, and NR were aliquoted and stored at −20°C.

Cell viability assays

Cells were plated at a density of 1,000 to 8,000 cells per well in 96-well plates and treated with NAMPTi 24 hours after plating. For rescue experiments, 10 μmol/L of NA was simultaneously administered with NAMPTi to cells during the treatment phase. Following 4 to 6 days of incubation, cells were fixed with 4% paraformaldehyde and stained with 1 μg/mL Hoechst 3342. Cells were imaged with a Cytation 3 (BioTek) and counted via CellProfiler (RRID: SCR_007358). Each experiment was conducted with at least three technical and biological replicates. Data were normalized to the vehicle-treated control group prior to analysis in GraphPad Prism software with a nonlinear regression analysis "inhibitor versus response—variable slope (four parameters)."

Cell viability assays on rhabdospheres were performed with CellTiter-Glo 2.0 (Promega). Rhabdospheres were plated with 10,000 cells per well in ultra-low attachment 96-well plates (Corning) and treated 24 hours later with NAMPTi, with and without NA concurrent supplementation, for 24 hours. CellTiter-Glo 2.0 (Promega) was performed per the manufacturer's specifications. The CellTiter-Glo assay was performed in three technical replicates.

PDX IncuCyte analysis

Real-time longitudinal cell proliferation was measured using the IncuCyte SX5 live-cell analysis system (Sartorius), with cell density and morphology imaged every 8 hours. The PDX-derived RMS cell line SJRHB013758 (FOXO1 fusion–negative) was plated at a density of 2,000 cells/well in 96-well plates. Cell culture conditions for this model have been previously described (25). Cells were allowed to adhere overnight and were treated the following day with doses of OT-82 (OncoTartis), NA (Sigma-Aldrich) at 10 μmol/L, or both. Each experiment was conducted 3 times with 12 technical replicates.

Apoptosis assays

Cells were plated at a density of 1.5×10^5 cells per well in 6-well plates and treated with DMSO, NA, NAMPTi, or concurrent NA and NAMPTi 24 hours after plating. After 48 hours of treatment, the Annexin V/propidium iodide (PI) apoptosis assay was performed using a Dead Cell Apoptosis Kit (Thermo Fisher Scientific) as per the manufacturer's specifications. The Annexin V/PI assay was performed in three technical replicates.

Cell-cycle analysis

Cells were plated at a density of 1.5×10^5 cells per well in six-well plates and treated with DMSO, NA, NAMPTi, or concurrent NA and NAMPTi 24 hours after plating. After 48 hours of treatment, cells were trypsinized and fixed dropwise with 70% ice-cold ethanol. Cells were then incubated with PI/RNase A stain (BD Biosciences) for 15 minutes at room temperature and analyzed through flow cytometry (Beckman Coulter Cytoflex LX).

Western blotting

Protein (40 μg/lane) was separated by 15% SDS-PAGE (Bio-Rad) and transferred onto PVDF membranes (Immobilon). Membranes were blocked with 5% nonfat skim milk for 1 hour at room temperature and then incubated with primary antibodies at 4°C overnight (Supplementary Table S1). Membranes were washed in TBS-T [20 mmol/L Tris (pH 7.5), 150 mmol/L NaCl, 0.1% Tween 20] and then incubated with secondary antibodies of horseradish peroxidase (HRP)–conjugated anti-mouse (Cell Signaling Technology, cat. #7076; PRID: AB_330924) or HRP-conjugated anti-rabbit (Cell Signaling Technology, cat. #7074; PRID: AB_2099233) for 1.5 hours at room temperature. Signals were visualized with an ECL Kit (Bio-Rad). Western blot quantification was performed using ImageJ software. After quantifying the band intensities of NAPRT and β-actin, NAPRT levels were normalized to β-actin for each clone and plotted against the corresponding OT-82 IC_{50} values, with and without NA.

NAD^+/NADH quantification

Cells were plated at 4,000 cells/well in 96-well plates and treated 24 hours later with NAMPTi, with and without NA concurrent supplementation, for 24 hours. The NAD/NADH-Glo Assay (Promega) was performed per the manufacturer's specifications. The NAD/NADH-Glo Assay was performed in three biological replicates.

In vivo studies (efficacy and NAD^+ quantification)

Animal studies were approved by Yale University's Institutional Animal Care and Use Committee protocol #2024-20071. Four- to six-week-old female Fox Chase SCID Beige mice (CB17.B6-Prkdc^{scid}Lyst bg/Cr) from Charles River Laboratories ($n = 3$–5 mice per treatment group) were used for cell line xenograft experiments. Two million cells were suspended in PBS and Matrigel (Corning) at a final volume of 100 μL and injected into the gastrocnemius muscle. Mice were randomized once the tumor was palpable. Mice were treated with vehicle (30% cyclodextrin), OT-82 (25 mg/kg), or OT-82 in combination with NA (25 mg/kg) by oral gavage daily, following a 3-day on and 4-day off treatment cycle for 5 weeks. Tumors were measured twice a week with calipers, and volume was calculated using the modified ellipsoid formula ($V = 0.5 \times L \times W^2$).

For patient-derived xenograft (PDX) propagation, RMS PDX models were obtained from St. Jude Children's Research Hospital as frozen cell stocks. Six- to eight-week-old female Athymic Nude-Foxn1nu mice from Envigo (PRID: IMSR_ENV:HSD-069; $n = 6$–9 mice per treatment group) were used for *in vivo* orthotopic PDX experiments. SJRHB010463_X16 cells (FOXO1 fusion–negative) were thawed, and a live cell count was obtained using trypan blue. One million cells were suspended in PBS and Matrigel at a final volume of 100 μL and injected into the gastrocnemius muscle for propagation. Once primary tumors reached a volume of ~2,000 mm^3, they were harvested, mechanically dissociated, and then passed through a 40 μm filter to achieve a single-cell suspension. These cells were then transplanted into the gastrocnemius muscle of new recipient mice for study purposes. Upon reaching a tumor volume of approximately 100 mm^3, mice were randomized into three treatment groups: Vehicle (30% cyclodextrin), OT-82 (25 mg/kg), and OT-82 + NA (25 mg/kg). Treatment strategy and tumor volume measurements were performed as described above.

For *in vivo* NAD^+ quantification, tumors and normal muscle were harvested from the mice 2 hours after one treatment cycle (i.e., after a 3-day "on" period of NAMPTi dosing). All tissues were snap-frozen. The NAD/NADH-Glo assay (Promega) was performed per the manufacturer's specifications. The NAD/NADH-Glo assay was performed in three technical replicates with 3 to 4 biological replicates per treatment group (Vehicle, NAMPTi, and NAMPTi + NA). NAD^+ concentration was normalized to the total mass of tissue (mg).

PDX tumor tissue microarray

PDX tissue microarrays (TMA) were constructed using formalin-fixed and paraffin-embedded PDX tissues. Paraffin sections from 29 pediatric RMS PDX models were stained with hematoxylin and eosin (H&E) to obtain a template guide slide for each tissue block and to validate sample quality and preservation. PDX samples with greater than 20% necrosis or inadequate tissue preservation were excluded. Slides were annotated to create a template for punching and were used as guides for PDX tumor core selection. Each array was designed using 0.6 mm diameter punches, with duplicates for each model. Tumor tissue cores from the 29 RMS PDX models were included in the arrays. Human (tonsil, testis, breast, colon, prostate, lung, kidney, and liver) and mouse (spleen, skin, colon, kidney, and liver) tissues were also included as controls.

Samples of patients with RMS

All research studies were conducted in accordance with US ethical guidelines (i.e., US Common Rule). Human tissue procurement and analysis procedures for specimens from patients with soft-tissue sarcoma were approved by the Institutional Review Board (IRB #2000027341) at Yale University. TMA slides containing samples of patients with RMS were also obtained from the National Cancer Trial Cooperative Network and the COG. Samples included in the TMAs were collected from patients enrolled in COG clinical trials D9602, D9802, and D9803, and these trials were approved by the IRB at each participating site. Written informed consent to participate in the study was provided by patients and/or their parents or guardians. The COG TMAs comprised 278 cores from 130 patients aged 0 to 18 years with both embryonal (FOXO1 fusion–negative) and alveolar (FOXO1 fusion–positive) tumors. Archived formalin-fixed, paraffin-embedded tissue was used to construct the TMA, with cores each measuring 1 mm in diameter. The presence of tumor was assessed via H&E staining. We excluded patients for whom only control cores and/or cores with insufficient tissue were present, resulting in a final analysis of 109 pediatric tumors.

NAPRT immunohistochemistry

The preparation of the TMA tissue for immunohistochemistry (IHC) was performed with an anti-NAPRT mouse mAb (4A5D7), developed and validated by Promab at Alphina Therapeutics (9). NAPRT IHC specificity and staining optimization were performed on cell line models and normal human tissue by NeoGenomics Laboratories using a Leica Bond III. Briefly, epitope retrieval was performed for 25 minutes at 100°C, blocked with Leica Protein Block for 30 minutes, and incubated with primary antibody (0.5 μg/mL) for 30 minutes. 3,3'-Diaminobenzidine was used for colorimetric detection. Samples were counterstained with hematoxylin. NAPRT signal was scored by a pathologist. The semiquantitative IHC scoring systems utilized were as follows: percentage positive score: (score = % positive cells) 0 = <1%; 1+ = 1% to 25%; 2+ = 25% to 50%; 3+ = 50% to 75%; 4+ = 75% to 100%.

DNA methylation analysis

Genomic DNA from 29 RMS tumors was analyzed using the Infinium MethylationEPIC BeadChip (Illumina). In addition, DNA methylation data from 70 RMS tumors previously generated on the Infinium HumanMethylation450 BeadChip were included in this analysis (dbGaP: phs001970; ref. 36). Raw IDAT files from both sources were processed and normalized using the swan algorithm in the minfi package (https://bioconductor.org/packages/release/bioc/html/minfi.html; refs. 37, 38). The β-value was computed as the measure of methylation, ranging from 0 (completely unmethylated) to 1 (completely methylated). The CpG probe annotation corresponding to the NAPRT1 gene was retrieved using the IlluminaHumanMethylationEPICanno.ilm10b2.hg19 package (https://bioconductor.org/packages/release/data/annotation/html/IlluminaHumanMethylationEPICanno.ilm10b2.hg19.html).

RNA sequencing and expression analysis

RNA sequencing data were available for 31 COG RMS samples, as previously described and available in the NCI Oncogenomics expression database (https://omics-oncogenomics.ccr.cancer.gov/cgi-bin/JK; refs. 39, 40). Briefly, RNA was extracted from samples using the QIAGEN RNeasy Micro Kits according to the manufacturer's protocol (QIAGEN). PolyA-selected RNA libraries were prepared for RNA sequencing on the Illumina HiSeq2000 using TruSeq v3 chemistry according to the manufacturer's protocol (Illumina). Hundred-base long paired-end reads were assessed for quality, and reads were mapped using the bcl2fastq tool in CASAVA (Illumina). Fastq files were mapped to the GRCh37 reference genome using the STAR alignment algorithm and quantified by the RSEM program based on Ensembl GRCh37.75 gene annotation (41, 42). Read counts were normalized using the trimmed mean of M-values method in edgeR and transformed to Fragments Per Kilobase of transcript per Million mapped reads (43).

Statistical analyses

A Student two-tailed *t* test was used for comparing two groups. One-way ANOVA with Dunnett's multiple comparison test was used to evaluate experiments involving one variable across multiple groups. Two-way ANOVA with the Tukey multiple comparison test was used to evaluate two variables across multiple groups. A log-rank test was performed to compare the survival of mice. Statistical significance was defined as $P < 0.05$. Statistical analyses were carried out using GraphPad Prism 10 software. All experiments were performed in biological triplicates unless noted otherwise.

Results

RMS models display NAPRT promoter methylation and low protein expression

We probed data from the Cancer Dependency Map (DepMap) to assess *NAPRT* promoter methylation and protein expression across different cancer types. High rates of *NAPRT* promoter methylation accompanied by low levels of NAPRT expression were observed in RMS cell line models (**Fig. 1B** and **C**). We then probed for NAPRT protein expression by immunoblot in a panel of RMS cell lines representing both FOXO1 fusion–negative (RD) and FOXO1 fusion–positive (RH28, RH30, and RH41) disease (44). We confirmed that a subset of models (RD and RH41) do not express NAPRT at the protein level, whereas NAMPT was detected in all cell lines (**Fig. 1D**).

NAPRT-deficient RMS cells show sensitivity to NAMPTi that is not reversed with NA supplementation

To determine whether NAPRT expression affects sensitivity to NAMPTi, RMS cells were treated for 96 hours with NAMPTi, with or without concurrent NA supplementation. RMS cells demonstrated marked sensitivity to FK-866, a first-generation small-molecule NAMPTi, and OT-82, a newer NAMPTi that has shown reduced cardiac, neurologic, and retinal toxicities in preclinical studies compared with earlier NAMPTi tested in clinical trials (34, 35). As expected, cells with a functional Preiss–Handler pathway driven by NAPRT expression (RH28 and RH30) were rescued by NA supplementation, whereas NAPRT-deficient cells (RD and RH41) exhibited no change in viability (**Fig. 1E–H**; Supplementary Fig. S1A–S1D).

Next, NAD^+ levels within RMS cell lines *in vitro* were quantified to better understand the mechanism underlying their sensitivity to NAMPTi. NAD^+ levels were assessed 24 hours after treatment with FK-866 or OT-82. Pools of NAD^+ dropped markedly in NAMPTi-treated cells that did not express NAPRT (RD and RH41), both in the absence and presence of NA, confirming their enhanced dependence on NAMPT activity for survival (**Fig. 1I** and **J**; Supplementary Fig. S1E and S1F). In contrast, NA supplementation fully restored NAD^+ levels after NAMPTi treatment in cells that expressed NAPRT (RH28 and RH30; **Fig. 1K** and **L**; Supplementary Fig. S1G and S1H). Finally, we evaluated the impact of OT-82 on normal human fibroblasts and mouse myoblasts (C2C12) in direct comparison with RMS cell lines. Interestingly, we found that both normal cell types, despite their different tissue origins, displayed substantially lower sensitivity to NAMPT inhibition (regardless of NAPRT expression), indicating a greater dependency of cancer cells on NAD^+ to support increased metabolic and biosynthetic demands, consistent with prior reports (Supplementary Fig. S1I and S1J; ref. 25).

To verify the on-target mechanism of NAMPTi and NAPRT-dependent rescue, we performed *in vitro* cell viability assays with the concurrent supplementation of NMN, NR, or NA. Nicotinamide is converted to NMN by NAMPT in the classical salvage pathway; therefore, regardless of NAPRT status, we would expect to observe rescue in cell viability (10). Similarly, NR is phosphorylated by NR kinase (NRK1/2) to form NMN upstream of NAMPT (10). As hypothesized, RH41 (NAPRT-deficient) and RH30 (NAPRT-expressing) were both rescued with coadministration of NMN and NR (Supplementary Fig. S2A, S2D, S2B, and S2E). However, when concurrently supplementing with NA, only RH30 was rescued following NAMPTi treatment (Supplementary Fig. S2C and S2F). To determine whether NA-mediated rescue was dose-dependent, we performed *in vitro* cell viability assays using NAPRT-expressing RH30 cells. We found that NA concentrations as low as 80 nmol/L, approximately 125-fold lower than the 10 μmol/L used throughout the article, were sufficient to rescue cells from NAMPTi-induced cytotoxicity (Supplementary Fig. S2G).

To confirm the dependence on NAPRT expression in mediating the NAMPTi response and rescue with NA, NAPRT was exogenously introduced into RH41 cells (**Fig. 2A**; Supplementary Fig. S3A) and RD cells (Supplementary Fig. S3D). Ectopic expression of NAPRT in RH41 ($RH41^{NAPRT+}$) and RD cells (RD^{NAPRT+}) rescued cell death with coadministration of NA, mirroring the effect of NAMPTi with NA supplementation in cells with endogenous NAPRT expression (RH28 and RH30; **Fig. 2B** and **C**; Supplementary Fig. S3B, S3C, and S3E). To further corroborate NAPRT-dependent sensitivity to NAMPTi with concurrent NA supplementation, we

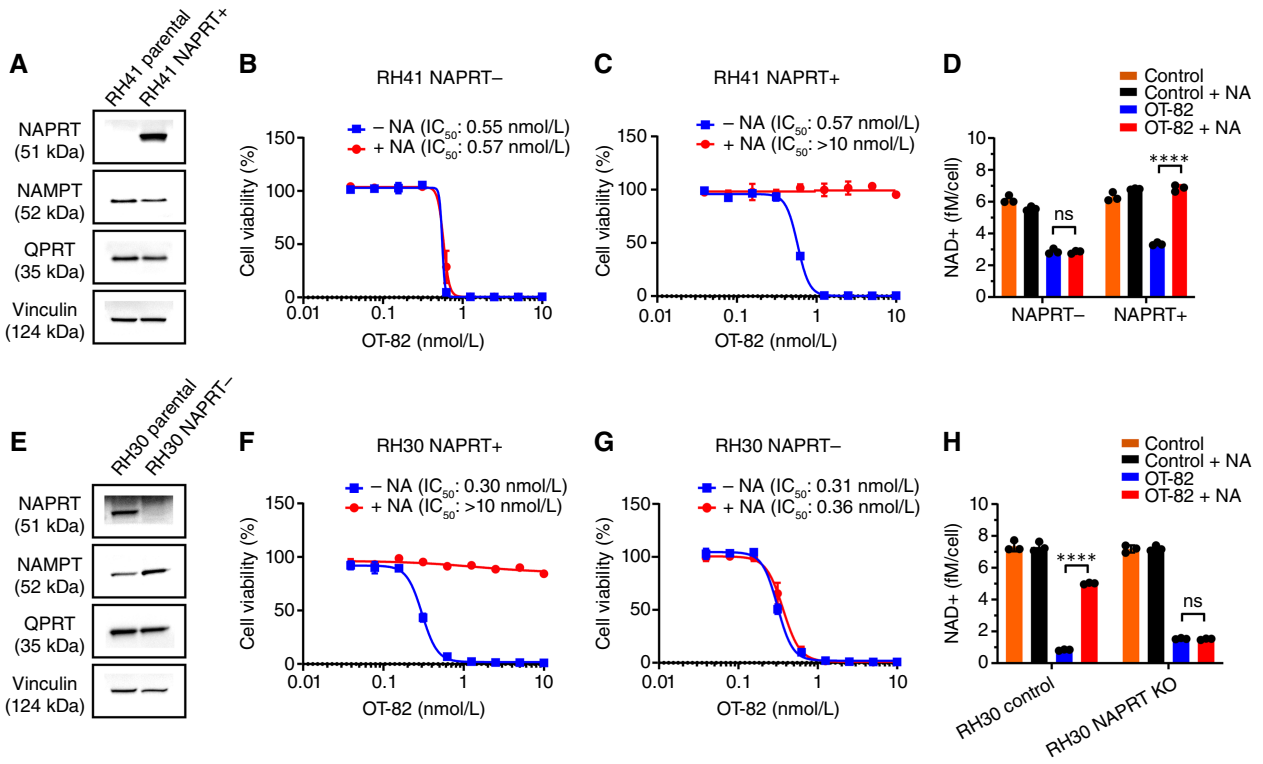

Figure 2.

Generation and functional validation of NAPRT isogenic models. **A–D,** Endogenously NAPRT-deficient RH41 cells transfected to ectopically express NAPRT ($RH41^{NAPRT+}$). **A,** Protein expression of NAPRT, NAMPT, QPRT, and vinculin in RH41 parental and $RH41^{NAPRT+}$. **B** and **C,** Cell viability in RH41 (NAPRT-deficient; **B**) and $RH41^{NAPRT+}$ (**C**) treated with increasing concentrations of OT-82 for 4 days with or without 10 μmol/L NA. **D,** Total NAD^+ quantification after 24 hours in RH41 (NAPRT-deficient) and $RH41^{NAPRT+}$ treated with respective IC_{50} concentration with or without 10 μmol/L NA. **E–H,** CRISPR/Cas9-mediated KO of NAPRT in endogenously NAPRT-expressing RH30 cells (RH30 NAPRT+). **E,** Protein expression of NAPRT, NAMPT, QPRT, and vinculin in RH30 parentals and RH30 NAPRT–. **F** and **G,** Cell viability in RH30 models treated with increasing concentrations of OT-82 for 4 days with or without 10 μmol/L NA. **H,** Total NAD^+ quantification after 24 hours in RH30 models treated with IC_{50} concentrations of OT-82 with or without 10 μmol/L NA. The data are plotted as means with error bars indicating SEM. ****, $P < 0.0001$; n.s., not significant.

performed CRISPR/Cas9-mediated knockout (KO) of *NAPRT* in naturally expressing RH30 cells ($RH30^{NAPRT-}$). KO of *NAPRT* was functionally validated via immunoblot, and cell proliferation assays demonstrated that $RH30^{NAPRT-}$ mimicked the effect of NAMPTi without NA rescue, as seen in endogenously NAPRT-deficient cells (**Fig. 2E–G**; Supplementary Fig. S4A–S4C). Furthermore, we conducted an additional *in vitro* analysis using our $RH30^{NAPRT-}$ isogenic model to assess how varying NAPRT expression levels influence cellular rescue in the presence of NA. Quantitative assessment of RH30 single-cell clones revealed that approximately 80% knockdown of NAPRT expression in RH30 WT cells abolished the NA-mediated rescue effect (Supplementary Fig. S4D). This suggests that maintaining ≥20% of wild-type NAPRT expression is preclinically sufficient to confer NA-dependent protection against NAMPT inhibition. Furthermore, NAD^+ levels were assessed in these isogenic models following a 24-hour NAMPTi treatment. Both FK866 and OT-82 significantly diminished the NAD^+ pool in both RH41 wild-type and $RH30^{NAPRT-}$, even with coadministration of NA, whereas $RH41^{NAPRT+}$ and RH30 wild-type were able to rescue their NAD^+ levels (**Fig. 2D** and **H**). Collectively, these data demonstrate that RMS cell lines are highly sensitive to NAMPT inhibition through NAD^+ depletion, with NA failing to rescue NAPRT-deficient cells, whereas NAPRT-expressing cells are protected by NA cotreatment.

NAMPT-mediated NAD^+ depletion leads to early-phase apoptosis in RMS cells

As we observed remarkable potency and a decrease in cellular proliferation following NAMPTi in RMS cells with a loss of NAPRT, we sought to decipher the mechanisms of cytotoxicity. Treatment with OT-82 induced only modest G_2–M arrest following 48 hours of NAMPTi treatment in RH41 (NAPRT-deficient); however, NAMPTi induced little to no arrest in RH30 (NAPRT-expressing) without NA supplementation (**Fig. 3A** and **B**; Supplementary Fig. S5A). Prior studies in various tumor types have indicated that early-phase apoptosis is observed following NAMPTi treatment (45). Most recently, in RMS, some models that exhibited full depletion of ATP following 72 to 120 hours of OT-82 treatment were shown to undergo necrosis (25). We treated RH41 and RH30 cells with OT-82 across multiple time points and concentrations. After 48 hours, the cleaved PARP1 signal was increased in both models across all concentrations of OT-82 (Supplementary Fig. S5B). Next, we treated RH41 and RH30 cells with OT-82 and concurrent NA supplementation for 48 hours. NAPRT-expressing cells lost the cleaved-PARP1 signal with the coadministration of NA (**Fig. 3C**). To further corroborate this observation that early apoptosis is ameliorated upon NA supplementation, we performed Annexin-V/PI staining at 48 hours of treatment. Supporting the

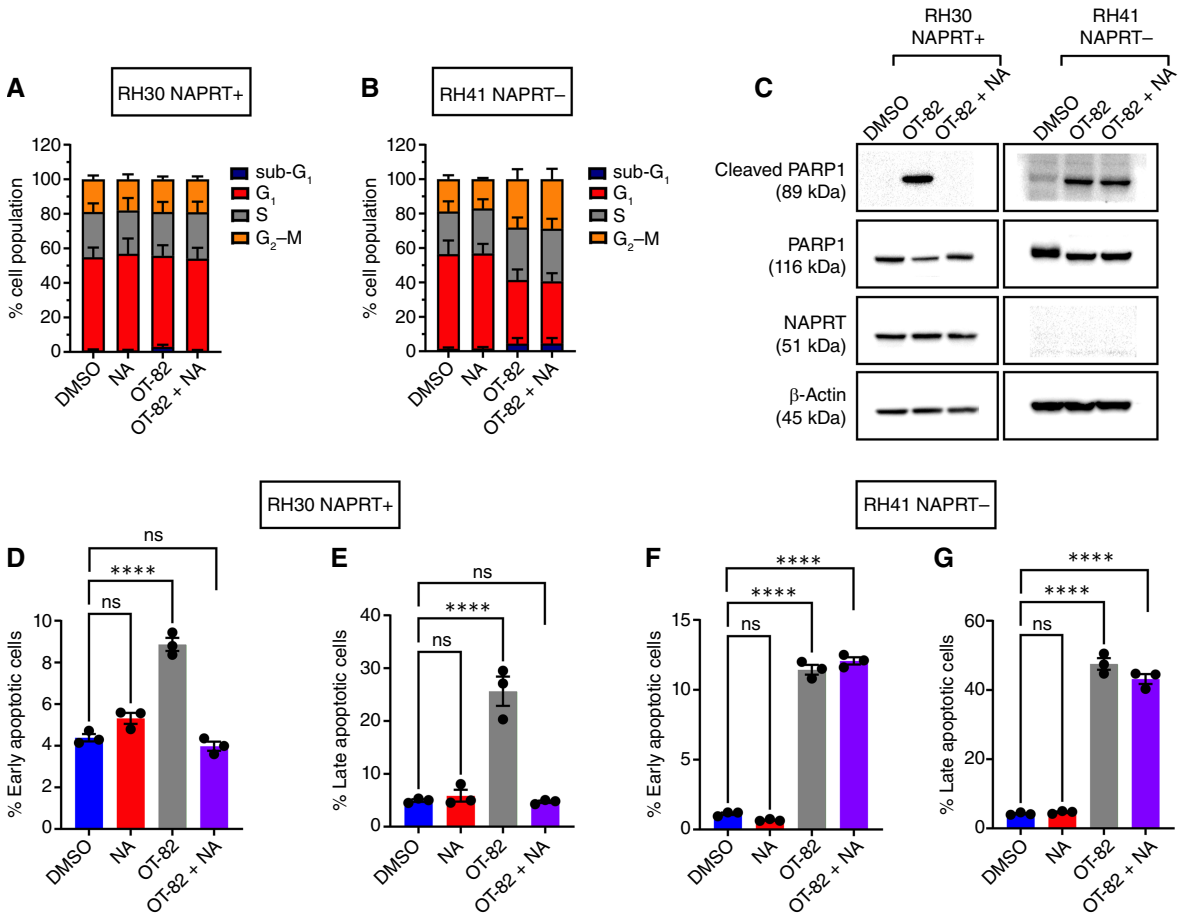

Figure 3.

NAMPTi induces early to late-phase apoptosis that is reversible with NA in NAPRT-expressing RMS models. **A** and **B,** Cell-cycle arrest after 48 hours of treatment with 0.1% DMSO, 10 μmol/L NA, 10 nmol/L OT-82, or the combination of OT-82 and NA in RH30 (NAPRT+; **A**) and RH41 (NAPRT−; **B**). **C,** Protein expression of cleaved PARP1, PARP1, NAPRT, and β-actin in RH30 (NAPRT+) and RH41 (NAPRT−) treated with DMSO, 10 nmol/L OT-82, or a combination of OT-82 and NA for 48 hours. **D–G,** Annexin-V/PI analysis after 48 hours of treatment with 0.1% DMSO, 10 μmol/L NA, 10 nmol/L OT-82, or the combination of OT-82 and NA on RH30 (NAPRT+; **D** and **E**) and RH41 (NAPRT−; **F** and **G**). The data represent the mean with error bars as SEM. ****, $P < 0.0001$; n.s., not significant.

immunoblot, in RH30 (NAPRT-expressing) cells, the induction of apoptosis was blunted when media was supplemented with NA (**Fig. 3D** and **E**; Supplementary Fig. S5C). Furthermore, in RH41 (NAPRT-deficient) cells, there was an increase in PI-positive, Annexin-V–positive, and double-positive (Annexin-V/PI-positive) events, indicating an induction of apoptosis in a subset of cells (**Fig. 3F** and **G**; Supplementary Fig. S5C). Collectively, these data demonstrate that RMS cell lines undergo early apoptosis. Notably, these assays were performed at concentrations above the IC_{50} values obtained from 4- to 6-day viability studies to account for a shorter incubation period, which may explain differences in cell death mechanisms compared with prior reports (25). Importantly, cell death induced by NAMPT inhibition is rescued by NA coadministration in NAPRT-expressing models.

NAMPTi demonstrates significant *in vivo* antitumor activity in RMS that is maintained with NA supplementation in NAPRT-negative models

To assess the efficacy of NAMPTi and NA coadministration in the context of endogenous NAPRT expression *in vivo*, we treated orthotopic RMS models bearing RH30 tumors. Following a clinical schedule used in early-phase trials, OT-82 was administered daily for 3 days on/4 days off at 25 mg/kg (35). Furthermore, 25 mg/kg of OT-82 and 25 mg/kg of NA were coadministered in the supplementation cohort. Notably, in endogenously NAPRT-expressing models, NA coadministration completely rescued cells from OT-82–mediated antitumor activity (**Fig. 4A** and **D**). Furthermore, tumor volumes from endogenously NAPRT-expressing models regressed following two cycles of treatment; however, we observed on-treatment progression after three cycles (**Fig. 4A** and **D**). Next, we performed *in vivo* studies with RH41 NAPRT isogenic pairs. Tumor regression was observed immediately after one cycle of OT-82 treatment in the mice bearing RH41 parental (NAPRT-deficient) tumors (**Fig. 4B**). Mice bearing $RH41^{NAPRT+}$ tumors experienced tumor regression after two cycles of OT-82 treatment (**Fig. 4C**). Survival was also improved in both RH41 parental and $RH41^{NAPRT+}$ tumors (**Fig. 4E** and **F**). Importantly, NA coadministration did not diminish the efficacy of OT-82 in RH41 parental (NAPRT-deficient) tumors, and $RH41^{NAPRT+}$ tumors exhibited no response to treatment

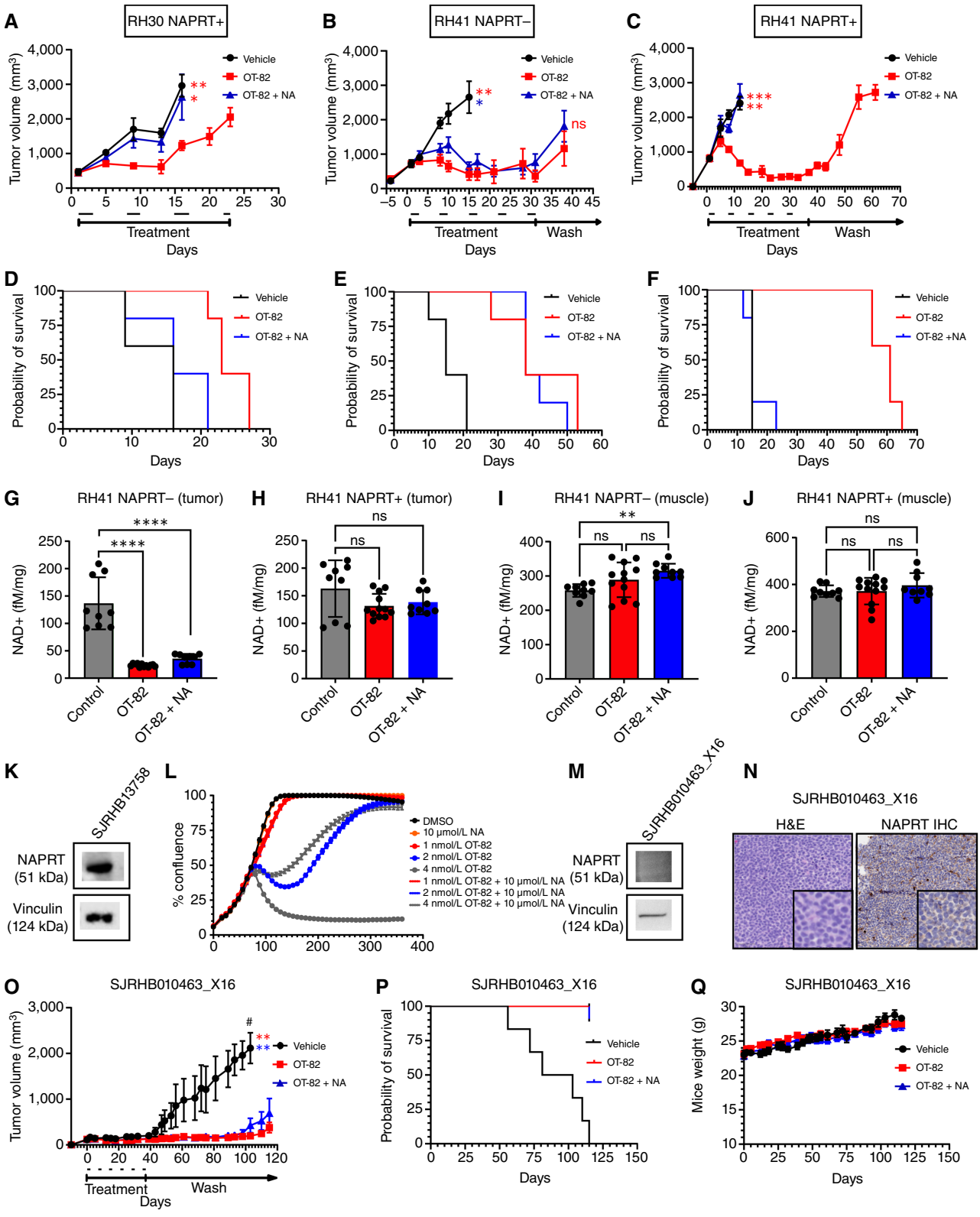

with NA coadministration (**Fig. 4B**, **C**, **E**, and **F**). Similar to the *in vitro* NA dose-titration experiment, a dose-dependent increase in rescue was observed in RH41 xenografts overexpressing NAPRT (Supplementary Fig. S6A). We did not observe any obvious toxicity, and mice maintained stable body weights in all three cohorts (Supplementary Fig. S6D–S6F). We analyzed tumor volumes after one treatment cycle, which entailed 3 days of treatment followed by 4 days of no treatment. RH41 (NAPRT-deficient) tumors demonstrated significant regression after one cycle of OT-82 alone or with NA supplementation. In contrast, no regression was observed in RH41^{NAPRT+} tumors after the same treatment cycle (Supplementary Fig. S6B). After two cycles, a clear separation in tumor volumes between control and OT-82–treated groups was evident in both NAPRT-deficient and NAPRT-expressing tumors (Supplementary Fig. S6C).

To corroborate this finding and assess the *in vivo* pharmacodynamic mechanism, total NAD^+ in tumor samples was measured following one cycle of OT-82 with and without NA coadministration in the RH41 NAPRT isogenic model. In RH41 (NAPRT-deficient) tumors, NAD^+ levels were significantly depleted after OT-82 treatment compared with vehicle control, even with exogenous NA administration (**Fig. 4G**). Interestingly, in RH41^{NAPRT+} tumors, there was not a statistically significant depletion of NAD^+ after treatment, regardless of NA administration, even though antitumor efficacy was observed with prolonged treatment (**Fig. 4H**). Additionally, we quantified NAD^+ pools in the contralateral normal muscle of both NAPRT-deficient and NAPRT-expressing tumor models after OT-82 treatment, with and without NA supplementation, and found no significant decrease in NAD^+ (**Fig. 4I** and **J**). This may suggest that the presence of NAPRT is protecting NAD^+ levels and viability in the presence of short-term NAMPTi treatment.

To further support our observation in cell-derived xenograft models, we profiled two RMS PDX models, SJRHB13758 and SJRHB010463_X16. SJRHB13758 was characterized as NAPRT-expressing via immunoblot (**Fig. 4K**). Consistent with this profile, SJRHB13758 exhibited *ex vivo* sensitivity to OT-82, an effect that was reversed by coadministration of NA via the functional Preiss–Handler pathway, at concentrations comparable with those effective in cell line models (**Fig. 4L**). In contrast, SJRHB010463_X16 was found to be NAPRT-deficient by immunoblot and IHC, making it an ideal model for *in vivo* evaluation of targeting NAPRT-deficient RMS tumors (**Fig. 4M** and **N**). Consistent with findings in isogenic models, OT-82 significantly suppressed tumor growth and prolonged survival compared with the vehicle control group, and this effect was not mitigated by NA supplementation. Notably, this sustained therapeutic effect persisted even several weeks after treatment cessation (**Fig. 4O–Q**). To investigate whether stem cell populations, which have been implicated in chemotherapy resistance, are similarly sensitive to NAD^+ depletion, we generated spheroids from NAPRT-deficient RH41 (32, 33). Following confirmation of stemness via SOX2 upregulation, these spheroids showed pronounced sensitivity to both FK-866 and OT-82, irrespective of NA supplementation (Supplementary Fig. S6G–S6J). These findings, together with the sustained regression observed in NAPRT-deficient PDX tumors, highlight the ability of this therapeutic approach to address the biological complexity of RMS, including the presence of treatment-resistant, stem-like cell populations.

NAPRT protein expression, methylation, and gene expression in samples of patients with RMS

To extend our findings into clinical samples, we next evaluated the loss of NAPRT expression at the protein level in patient tumor samples via IHC staining using a newly validated NAPRT mAb (4A5D7; ref. 9). First, we probed a pilot TMA generated at our institution consisting of 33 human RMS samples. Based on a semiquantitative scoring system accounting for the percentage of positive tumor cells, 28% of RMS samples demonstrated loss of NAPRT protein expression, classified as <1% of tumor cells showing any cytoplasmic or nuclear staining (**Fig. 5A**; Supplementary Table S2). Next, we performed IHC staining in a TMA generated from RMS PDX models representing a total of 29 unique patients and again observed loss of NAPRT protein expression in roughly 30% of samples (**Fig. 5B**; Supplementary Table S3). No significant difference in the frequency of NAPRT loss was observed across histologic subtypes or by FOXO1 fusion status in either the pilot patient cohort or the PDX TMA (**Fig. 5C**; Supplementary Fig. S7A and S7B). To corroborate these findings in a larger cohort of samples, we performed IHC staining in multiple validated TMAs previously generated from pediatric patients with RMS enrolled in COG clinical trials (Supplementary Table S4). The COG TMAs consisted of samples from a total of 109 patients aged 0 to 18 years. Using the same semiquantitative scoring system utilized in the pilot TMA study, approximately 40% of pediatric RMS samples demonstrated loss of NAPRT protein expression (**Fig. 5D**; Supplementary Fig. S7C). Again, NAPRT protein loss did not significantly differ by histologic subtype or FOXO1 fusion status (**Fig. 5E** and **F**). Examination of clinical data from patients with total loss of NAPRT revealed a higher proportion of male patients, with a predominance of tumors arising in genitourinary sites (Supplementary Fig. S7D

Figure 4.

OT-82 leads to delayed tumor growth, prolonged survival, and decreased NAD^+ levels that are not rescued with NA in NAPRT-deficient xenograft models. **A–F,** Tumor growth curves (**A–C**) and Kaplan–Meier plots (**D–F**) of Fox Chase SCID mice bearing RH30 (NAPRT+; **A** and **D**), RH41 (NAPRT−; **B** and **E**), and RH41^{NAPRT+} (**C** and **F**), following treatment with 30% cyclodextrin vehicle, 25 mg/kg OT-82, and 25 mg/kg OT-82 in combination with 25 mg/kg NA. **G** and **H,** Total NAD^+ levels in tumors harvested from RH41 (NAPRT−; **G**) and RH41^{NAPRT+} (**H**) models treated with one cycle of 30% cyclodextrin vehicle, 25 mg/kg OT-82, and 25 mg/kg NAMPTi in combination with 25 mg/kg NA. **I** and **J,** Total NAD^+ levels in contralateral normal gastrocnemius muscle harvested from RH41 (NAPRT−; **I**) and RH41^{NAPRT+} (**J**) treated with one cycle of 30% cyclodextrin vehicle, 25 mg/kg OT-82, and 25 mg/kg NAMPTi in combination with 25 mg/kg NA. For **G–J**, each treatment cohort included three biological replicates, with two technical replicates per biological replicate. **K,** NAPRT expression by Western blot in the NAPRT-expressing PDX model (SJRHB13758). **L,** Cell viability in SJRHB13758 treated with increasing concentrations of OT-82 with and without 10 μmol/L NA. **M,** NAPRT expression by Western blot in the PDX model, SJRHB010463_X16, confirming NAPRT deficiency. **N,** Representative NAPRT IHC (left) and H&E (right) images of SJRHB010463_X16, a NAPRT-deficient PDX model. **O–Q,** Tumor growth curves (**O**), Kaplan–Meier plots (**P**), and body weight plots (**Q**) of 6- to 8-week-old female Athymic Nude-Foxn1nu mice bearing RMS PDX SJRHB010463_X16. For **A–F**, each treatment group had five biological replicates (control $N = 5$; OT-82 $N = 5$; and OT-82 + NA $N = 5$). For **O–Q**, each group had 6–9 biological replicates (control $N = 6$; OT-82 $N = 8$; and OT-82 + NA $N = 9$). The data are plotted as means with error bars indicating SEM. *, $P < 0.05$; **, $P < 0.01$; ***, $P < 0.001$; ****, $P < 0.0001$; n.s., not significant. # represents that tumors in >50% of the mice in the vehicle group reached humane end-point. Therefore, mice were euthanized and dropped out of the study.

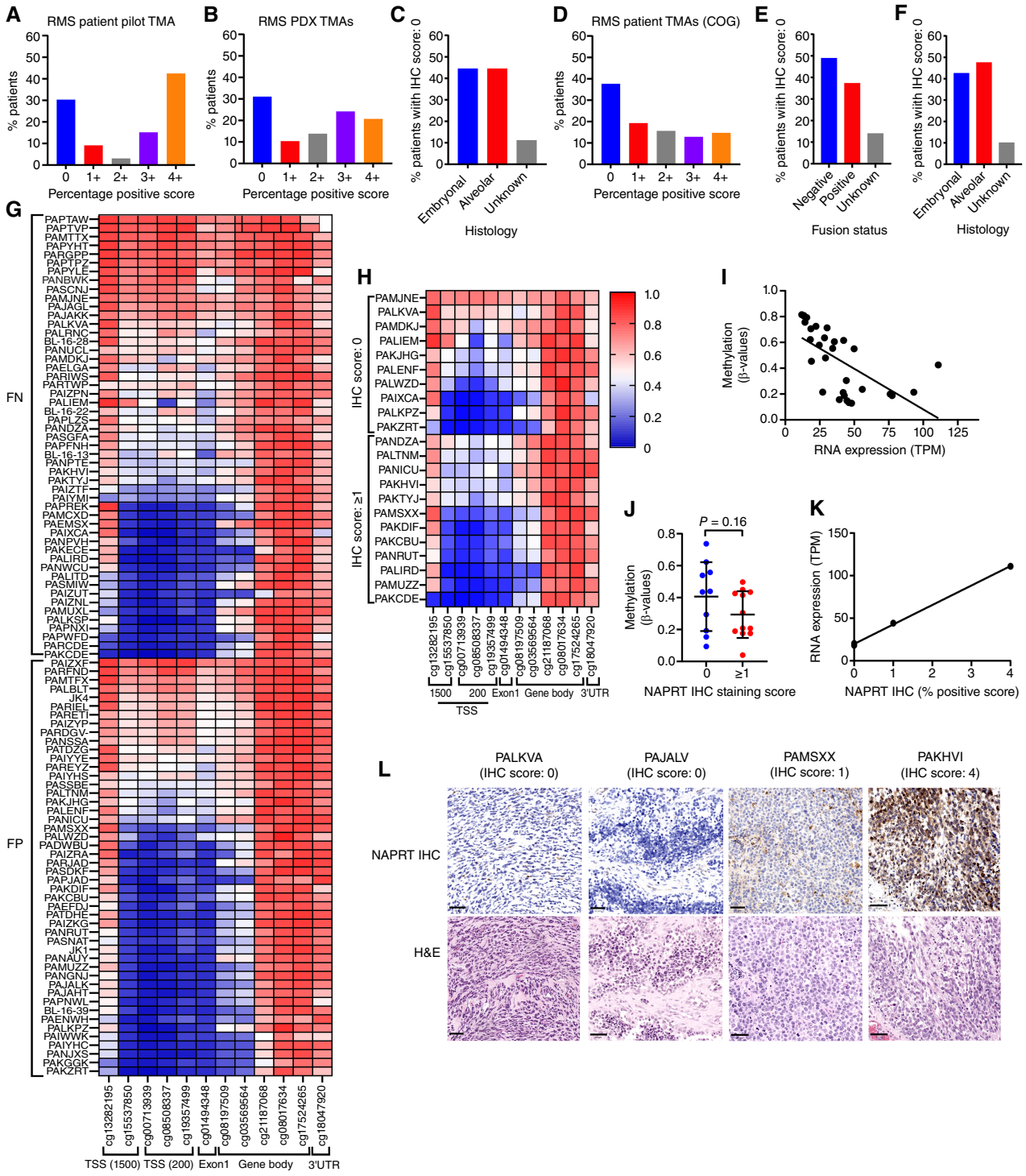

Figure 5.

Loss of NAPRT expression in samples of patients with RMS. **A,** Summary of NAPRT IHC score in pilot TMA ($n = 33$ individual patients) using a semiquantitative scoring system based on the percentage of positive tumor cells. **B** and **C,** Summary of NAPRT IHC score in PDX TMA ($n = 29$ individual RMS PDX) by percentage of positive tumor cells (**B**) and by histology (**C**). **D–F,** Summary of NAPRT IHC score in COG TMAs ($n = 109$ individual patients) by percentage of positive tumor cells (**D**), fusion status (**E**), and histology (**F**). **G,** Heatmap representing methylation β-values of 12 CpG probes corresponding to the NAPRT1 gene (*x*-axis) of 99 pediatric patients with RMS from COG TMA, stratified by fusion status (*y*-axis). **H,** Heatmap of 22 pediatric patients with RMS with corresponding IHC and methylation data, stratified by total protein loss (top; IHC score = 0) or the presence of NAPRT protein (bottom; IHC score ≥1). **I,** Inverse relationship between RNA expression (TPM) and methylation β-values at the TSS 200 and 1,500 of 31 patients with RMS ($r^2 = 0.38$). **J,** Graph (*Continued on the following page.*)

and S7E). No significant associations were observed with tumor stage or metastatic status (Supplementary Fig. S7F–S7K).

Because *NAPRT* promoter methylation has been implicated as a driver of epigenetic silencing, we sought to correlate methylation with transcription and protein expression (9, 26, 29, 46, 47). We analyzed previously generated methylation data from 99 samples of patients with RMS through the COG. Consistent with our findings in cell line models, we observed that a subset of RMS harbors hypermethylation of the *NAPRT* promoter across both FOXO1 fusion–positive and FOXO1 fusion–negative tumors (**Fig. 5G**). Of the COG samples with available methylation data, 31 had corresponding RNA sequencing data, and 22 had corresponding tissue in the TMA for IHC staining (**Fig. 5H**). We observed an inverse correlation between the average methylation β-values at the transcriptional start site 200 (TSS200) and TSS1500 regions of the *NAPRT* promoter with gene expression, as measured by transcript per million (TPM; **Fig. 5I**). Interestingly, there was a trend toward higher average methylation β-values at TSS regions in samples with complete loss of NAPRT protein staining compared with those with any positive staining, although this did not reach statistical significance (**Fig. 5J**). Only four patients had corresponding transcriptomic and IHC data, which demonstrated a positive correlation between NAPRT gene expression and protein staining, despite the limited sample size (**Fig. 5K** and **L**).

Discussion

RMS remains a major therapeutic challenge, particularly in high-risk patients where there is a high unmet need for novel treatments to improve survival. Consistent with emerging evidence in pediatric bone and soft-tissue sarcomas, our findings demonstrate that RMS is highly vulnerable to NAMPT inhibition (25). Importantly, we build upon this foundational work by providing the first comprehensive analysis of NAPRT expression in pediatric RMS, leveraging patient-derived tumor samples, preclinical *in vivo* models, and isogenic cell line systems.

Probing methylation data within the DepMap, we found a high frequency of *NAPRT* gene promoter hypermethylation in RMS models. Our *in vitro* data show that NAPRT-deficient RMS cells are incapable of utilizing the Preiss–Handler pathway for NAD^+ biosynthesis, and their survival is dependent on NAMPT activity. NAMPTi treatment led to profound cytotoxicity and NAD^+ depletion in these cells, effects that were not reversed with NA supplementation. In contrast, NAPRT-proficient RMS cells were rescued from NAMPTi-induced cytotoxicity with NA. *In vivo*, NAMPTi alone and with NA induced significant tumor regression in both endogenous and engineered NAPRT-deficient orthotopic RMS xenograft models. Notably, contrary to some prior reports, NA coadministration did not abrogate antitumor efficacy in NAPRT-deficient tumors but did preserve NAD^+ levels and reversed antitumor efficacy in NAPRT-positive tissues (48). Interestingly, in $RH41^{NAPRT+}$ tumors, there was no statistically significant depletion of NAD^+ after one cycle of OT-82 treatment compared with RH41 parental (NAPRT-deficient) tumors. This corresponded with the observation that RH41 parental tumors demonstrated significant regression after one cycle with or without NA supplementation, whereas no regression was observed in $RH41^{NAPRT+}$ tumors at the same time point, even though robust antitumor efficacy was ultimately observed in both models with prolonged treatment. These data may suggest that NAPRT expression alters the kinetics of NAD^+ depletion and cytotoxicity *in vivo*.

Based on these findings, our study supports the feasibility of a "protective rescue" paradigm, in which cotreatment with NA could expand the therapeutic window of NAMPTi, potentially overcoming dose-limiting toxicities noted in preclinical and early-phase clinical trials (9, 13, 26, 45, 49). Based on the dose conversion between animals and humans [Human Equivalent Dose (mg/kg) = animal dose (mg/kg) × Km ratio (animal/human)], our dose of 25 mg/kg of NA supplementation for our *in vivo* studies in mice is approximately 2 mg/kg for humans, a dose well within the limits of safe daily NA intake (50). Importantly, dietary intake of NA has not been controlled for in previous clinical trials and may have contributed to the lower-than-expected efficacy of NAMPTi by inadvertently rescuing NAPRT-expressing tumors. Prospective selection of NAPRT-deficient tumors could mitigate this confounder and improve therapeutic outcomes. Further pharmacokinetic and pharmacodynamic studies are warranted to characterize the NAD^+ metabolome within the tumor microenvironment and to optimize NA dosing for future clinical translation of this therapeutic approach.

To further establish the translational relevance of *NAPRT* silencing in RMS, we evaluated promoter methylation, gene expression, and protein levels across multiple patient cohorts. Our findings demonstrate that a sizable subset of RMS tumors exhibit *NAPRT* promoter hypermethylation, with approximately 30% to 40% of cases harboring loss of NAPRT protein expression. Although promoter methylation is strongly implicated in *NAPRT* silencing, the modest correlation between methylation and protein loss observed in tumors of patients with RMS suggests additional regulatory mechanisms may be involved. These could include histone modifications, posttranscriptional regulation, or structural variants disrupting the *NAPRT* locus. Of note, our study is limited by the relatively small number of patient samples with matched protein, methylation, and transcriptomic data, restricting our ability to build a robust classifier for NAPRT status. Further investigation is warranted to determine the optimal cutoff of NAPRT expression and to refine biomarker-based patient selection strategies for future clinical trials. In addition, the heterogeneity of NAPRT expression within and between tumors warrants additional study, particularly in the context of potential clonal evolution under selective pressure from NAMPTi therapy.

NAPRT silencing has also been reported in diffuse intrinsic pontine glioma and glioblastoma, as well as fumarate hydratase–deficient renal carcinoma, due to varying epigenetic mechanisms (9, 29). Evolutionarily, it is not well understood why some tumors prefer to rely on a specific NAD^+ biosynthesis pathway and repress another. Interestingly, one study investigated the inherent loss of NAPRT through a tissue lineage–based hypothesis, suggesting that tumors arising from normal tissues that do not depend on the Priess–Handler pathway, and therefore NAPRT, are more dependent on the NAMPT-mediated salvage pathway (51). Intriguingly, skeletal muscle cells have been indicated as non-Priess–Handler pathway–dependent

(*Continued*.) showing a negative correlation trend of β-values at TSS200 and TSS1500 regions with NAPRT IHC score for 22 patients in **H**. **K,** Correlation between COG TMA NAPRT IHC score and RNA expression of four patients ($r^2 = 0.99$). **L,** Representative NAPRT IHC (top) and H&E (bottom) images in patients with corresponding IHC and transcriptomic data. In **A**, **B**, and **D**, percentage positive score: (score = % positive cells) 0 = <1%; 1+ = 1%–25%; 2+ = 25%–50%; 3+ = 50%–75%; 4+ = 75%–100%.

(51). As a tumor that may arise from dysregulation in skeletal muscle differentiation, the tissue lineage–based hypothesis may provide an explanation for NAPRT silencing in RMS.

Furthermore, NAMPT plays an important role in mediating the downstream function of NAD^+-dependent enzymes that influence multiple aspects of cancer biology. Among these, poly-ADP ribose polymerases (PARP) are major consumers of NAD^+ as it functions as an important substrate needed for PARP to form poly (ADP-ribose) chains, which recruit DNA damage response proteins. As such, previous studies have reported synergy between PARP inhibitors and NAMPTi (9, 29, 52). Moreover, cotreatment with temozolomide and NAMPTi has shown additive effects in preclinical glioma models, attributed to a "hypervulnerability" secondary to NAD^+ depletion from PARP1 activation (53). Exploring combination strategies that pair NAMPTi with DNA-damaging agents or DNA repair inhibitors represents an important future direction for clinical translation that bridges tumor metabolism and genomic instability, with careful optimization of sequencing, timing, and dosing being important for maximizing therapeutic efficacy and tolerability. Additionally, resistance to NAMPT inhibition has been reported through multiple mechanisms, including intrinsic or adaptive alterations in NAD^+ biosynthesis pathways such as upregulation of NAPRT, metabolic rewiring that reduces cellular dependence on NAD^+, and acquisition of NAMPT mutations that diminish inhibitor binding (54). Further investigation of these resistance mechanisms will be important for improving response durability and informing the clinical development of NAMPTi.

In conclusion, we identify NAPRT loss as a frequent and functionally relevant event in RMS that can be exploited therapeutically through NAD^+ depletion with NAMPTi. Our work has important implications for the design of future clinical trials of NAMPTi in pediatric cancers. First, routine assessment of NAPRT status, via IHC or methylation analysis, could enable the selection of patients most likely to benefit from NAMPTi monotherapy. Second, in patients with NAPRT-expressing tumors, NA coadministration may allow dose escalation while reducing off-target toxicities. Overall, these findings support further clinical study of NAMPTi in RMS via biomarker-driven clinical trials and rational combination therapies aimed at overcoming resistance and minimizing toxicity.

Data Availability

The COG TMA patient methylation data (dbGaP: phs001970) analyzed in this study are available and were analyzed in collaboration with the authors of the original publication, Sun and colleagues (36). The RNA sequencing and expression data are publicly available in the NCI Oncogenomic expression database (https://omics-oncogenomics.ccr.cancer.gov/cgi-bin/JK) and were analyzed in collaboration with the authors of the original publications, Shern and colleagues and Brohl and colleagues (39, 40). Further analysis information pertaining to methylation and RNA expression analysis can be found in "DNA methylation analysis" and "RNA sequencing and expression analysis" above, respectively. All noncommercial materials are available upon request. No other data were created and analyzed in this study.

Authors' Disclosures

K.J. Noronha reports grants from the NIH during the conduct of the study, as well as personal fees from AtlasXomics Inc. outside the submitted work. F.G. Barr reports grants from the Joanna McAfee Childhood Cancer Foundation during the conduct of the study; and Abbott Laboratories, Bristol Myers Squibb Co., Eli Lilly and Company, Johnson & Johnson, Labcorp Holdings Inc., UnitedHealth Group Inc., Edwards Lifesciences. J.-S. Yi reports other support from Alphina Therapeutics during the conduct of the study. C. Brenner reports other support from Alphina Therapeutics outside the submitted work and a patent for US20210369681A1 issued to Alphina Therapeutics. C.D. Heer reports grants from the NCI during the conduct of the study. J.C. Vasquez reports grants from Hyundai Hope on Wheels, NCI/NIH K08, and the Robert Wood Johnson Harold Amos Medical Faculty Development Program during the conduct of the study. No disclosures were reported by the other authors.

Authors' Contributions

A. Kim: Data curation, formal analysis, investigation, writing–original draft, writing–review and editing. **P. Bhardwaj:** Data curation, formal analysis, investigation, visualization, writing–original draft, writing–review and editing. **S. Rehman:** Investigation, writing–review and editing. **S.J. Zhao:** Investigation, writing–original draft. **K.N. Lucas:** Investigation. **K.J. Noronha:** Investigation, writing–review and editing. **D. Bhatt:** Data curation, investigation. **S. Friedman:** Visualization, methodology. **R. Morotti:** Data curation, investigation, writing–review and editing. **R.K. Sundaram:** Formal analysis, investigation, writing–review and editing. **F.S. Dela Cruz:** Resources, writing–review and editing. **T.Y. Feinberg:** Resources, writing–review and editing. **S. Ramakrishnan:** Data curation, writing–review and editing. **W. Xue:** Data curation, writing–review and editing. **D.A. Barkauskas:** Data curation, writing–review and editing. **D. Hall:** Data curation, writing–review and editing. **J.F. Shern:** Data curation, investigation, visualization, writing–review and editing. **W. Sun:** Data curation, investigation, writing–review and editing. **F.G. Barr:** Data curation, investigation, writing–review and editing. **J.-S. Yi:** Methodology, writing–review and editing. **J. Spurrier:** Data curation, methodology, writing–review and editing. **A. Yu:** Investigation. **C. Brenner:** Conceptualization, writing–review and editing. **C.D. Heer:** Data curation, visualization, writing–review and editing. **C.M. Heske:** Investigation, writing–original draft, writing–review and editing. **J.C. Vasquez:** Conceptualization, resources, supervision, funding acquisition, writing–original draft, writing–review and editing.

Acknowledgments

The authors would like to thank Drs. Ranjit S. Bindra, Douglas Spitz, and Ranjithmenon Muraleedharan for their support in the conceptualization of the study and NAD^+ metabolism expertise. The authors also thank Mitch Raponi and Marc Damelin from Alphina Therapeutics for providing anti-NAPRT antibodies for IHC staining and for their expertise in the development of companion diagnostics. Furthermore, we would like to show our appreciation to Dr. Keiichiro Tanaka from Alphina Therapeutics for his bioinformatics expertise. The authors also thank Dr. Corinne Linardic for providing the RH28 cell line. A. Kim is supported by the Yale Cancer Biology Training Program (5T32CA193200-09). P. Bhardwaj is supported by NIH grant. C.D. Heer is supported by the NIH/NCI award (K00CA245722). J.C. Vasquez is supported in part by the NIH/NCI award (1K08CA258796), the Hyundai Hope on Wheels Scholar Hope Grant, the Robert Wood Johnson Harold Amos Medical Faculty Development Program, the Fund to Retain Clinical Scientists at Yale, sponsored by the Doris Duke Charitable Foundation award #2015216, and the Yale Center for Clinical Investigation, and by an American Cancer Society Institutional Research Grant, #IRG-21-132-60-IRG. This work was also supported by grants from the NCI, NIH to the COG (U10CA180886, U24CA196173, U10CA180899). J.F. Shern, F.G. Barr, and C.M. Heske were supported by the Intramural Research Program of the NCI. We thank the Yale Center for Genome Analysis and the Yale Keck Biotechnology Core for their assistance. The results shown here are in part based on data from the DepMap (https://depmap.org). We thank Yale Flow Cytometry for their assistance with their service. The Core is supported in part by an NCI Cancer Center Support Grant # NIH P30 CA016359. We thank the Yale Tissue Pathology Services Core for their assistance in generating tumor TMAs. The authors would like to acknowledge the Childhood Solid Tumor Network at St. Jude for providing PDX models. The content is solely the responsibility of the authors and does not necessarily represent the official views of the NIH. During the preparation of this manuscript, generative artificial intelligence tools were used solely to assist with language editing, including improving clarity, grammar, and readability of text originally written by the authors. These tools were not used to generate scientific content, data, figures, analyses, or references. All scientific content, interpretations, and conclusions were developed entirely by the authors, who reviewed and take full responsibility for the final manuscript.

Note

Supplementary data for this article are available at Molecular Cancer Therapeutics Online (http://mct.aacrjournals.org/).

Received June 3, 2025; revised February 27, 2026; accepted April 13, 2026; posted first April 22, 2026.

References

1. Dasgupta R, Fuchs J, Rodeberg D. Rhabdomyosarcoma. Semin Pediatr Surg 2016;25:276–83.
2. Malempati S, Hawkins DS. Rhabdomyosarcoma: review of the Children's Oncology Group (COG) Soft-Tissue Sarcoma Committee experience and rationale for current COG studies. Pediatr Blood Cancer 2012;59:5–10.
3. Yohe ME, Heske CM, Stewart E, Adamson PC, Ahmed N, Antonescu CR, et al. Insights into pediatric rhabdomyosarcoma research: challenges and goals. Pediatr Blood Cancer 2019;66:e27869.
4. Metts JL, Aye JM, Crane JN, Oberoi S, Balis FM, Bhatia S, et al. Roadmap for the next generation of Children's Oncology Group rhabdomyosarcoma trials. Cancer 2024;130:3785–96.
5. Cantó C, Menzies KJ, Auwerx J. NAD(+) metabolism and the control of energy homeostasis: a balancing act between mitochondria and the nucleus. Cell Metab 2015;22:31–53.
6. Kalhan SC, Hanson RW. Resurgence of serine: an often neglected but indispensable amino acid. J Biol Chem 2012;287:19786–91.
7. Chiarugi A, Dölle C, Felici R, Ziegler M. The NAD metabolome–a key determinant of cancer cell biology. Nat Rev Cancer 2012;12:741–52.
8. Heske CM. Beyond energy metabolism: exploiting the additional roles of NAMPT for cancer therapy. Front Oncol 2019;9:1514.
9. Noronha KJ, Lucas KN, Paradkar S, Edmonds J, Friedman S, Murray MA, et al. NAPRT silencing in FH-deficient renal cell carcinoma confers therapeutic vulnerabilities via NAD+ depletion. Mol Cancer Res 2024;22:973–88.
10. Belenky P, Bogan KL, Brenner C. NAD+ metabolism in health and disease. Trends Biochem Sci 2007;32:12–9.
11. Nahimana A, Attinger A, Aubry D, Greaney P, Ireson C, Thougaard AV, et al. The NAD biosynthesis inhibitor APO866 has potent antitumor activity against hematologic malignancies. Blood 2009;113:3276–86.
12. Gehrke I, Bouchard EDJ, Beiggi S, Poeppl AG, Johnston JB, Gibson SB, et al. On-target effect of FK866, a nicotinamide phosphoribosyl transferase inhibitor, by apoptosis-mediated death in chronic lymphocytic leukemia cells. Clin Cancer Res 2014;20:4861–72.
13. Lee J, Kim H, Lee JE, Shin S-J, Oh S, Kwon G, et al. Selective cytotoxicity of the NAMPT inhibitor FK866 toward gastric cancer cells with markers of the epithelial-mesenchymal transition, due to loss of NAPRT. Gastroenterology 2018;155:799–814.e13.
14. Xiao Y, Elkins K, Durieux JK, Lee L, Oeh J, Yang LX, et al. Dependence of tumor cell lines and patient-derived tumors on the NAD salvage pathway renders them sensitive to NAMPT inhibition with GNE-618. Neoplasia 2013;15:1151–60.
15. Goldinger SM, Gobbi Bischof S, Fink-Puches R, Klemke C-D, Dréno B, Bagot M, et al. Efficacy and safety of APO866 in patients with refractory or relapsed cutaneous T-cell lymphoma: a phase 2 clinical trial. JAMA Dermatol 2016;152:837–9.
16. Holen K, Saltz LB, Hollywood E, Burk K, Hanauske A-R. The pharmacokinetics, toxicities, and biologic effects of FK866, a nicotinamide adenine dinucleotide biosynthesis inhibitor. Invest New Drugs 2008;26:45–51.
17. von Heideman A, Berglund A, Larsson R, Nygren P. Safety and efficacy of NAD depleting cancer drugs: results of a phase I clinical trial of CHS 828 and overview of published data. Cancer Chemother Pharmacol 2010;65:1165–72.
18. Misner DL, Kauss MA, Singh J, Uppal H, Bruening-Wright A, Liederer BM, et al. Cardiotoxicity associated with nicotinamide phosphoribosyltransferase inhibitors in rodents and in rat and human-derived cells lines. Cardiovasc Toxicol 2017;17:307–18.
19. Cassar S, Dunn C, Olson A, Buck W, Fossey S, Ramos MF, et al. From the cover: inhibitors of nicotinamide phosphoribosyltransferase cause retinal damage in larval zebrafish. Toxicol Sci 2018;161:300–9.
20. Zabka TS, Singh J, Dhawan P, Liederer BM, Oeh J, Kauss MA, et al. Retinal toxicity, in vivo and in vitro, associated with inhibition of nicotinamide phosphoribosyltransferase. Toxicol Sci 2015;144:163–72.
21. Mutz CN, Schwentner R, Aryee DNT, Bouchard EDJ, Mejia EM, Hatch GM, et al. EWS-FLI1 confers exquisite sensitivity to NAMPT inhibition in Ewing sarcoma cells. Oncotarget 2017;8:24679–93.
22. Heske CM, Davis MI, Baumgart JT, Wilson K, Gormally MV, Chen L, et al. Matrix screen identifies synergistic combination of PARP inhibitors and nicotinamide phosphoribosyltransferase (NAMPT) inhibitors in ewing sarcoma. Clin Cancer Res 2017;23:7301–11.
23. Gibson AE, Yeung C, Issaq SH, Collins VJ, Gouzoulis M, Zhang Y, et al. Inhibition of nicotinamide phosphoribosyltransferase (NAMPT) with OT-82 induces DNA damage, cell death, and suppression of tumor growth in preclinical models of Ewing sarcoma. Oncogenesis 2020;9:80.
24. Piacente F, Caffa I, Ravera S, Sociali G, Passalacqua M, Vellone VG, et al. Nicotinic acid phosphoribosyltransferase regulates cancer cell metabolism, susceptibility to NAMPT inhibitors, and DNA repair. Cancer Res 2017;77:3857–69.
25. McKay-Corkum GB, Collins VJ, Yeung C, Ito T, Issaq SH, Holland D, et al. Inhibition of NAD+-dependent metabolic processes induces cellular necrosis and tumor regression in rhabdomyosarcoma models. Clin Cancer Res 2023;29:4479–91.
26. Franceschini N, Oosting J, Tamsma M, Niessen B, Bruijn IB, van den Akker B, et al. Targeting the NAD salvage synthesis pathway as a novel therapeutic strategy for osteosarcomas with low NAPRT expression. Int J Mol Sci 2021;22:6273.
27. Zhang P, Brinton LT, Williams K, Sher S, Orwick S, Tzung-Huei L, et al. Targeting DNA damage repair functions of two histone deacetylases, HDAC8 and SIRT6, sensitizes acute myeloid leukemia to NAMPT inhibition. Clin Cancer Res 2021;27:2352–66.
28. Peterse EFP, van den Akker BEWM, Niessen B, Oosting J, Suijker J, de Jong Y, et al. NAD synthesis pathway interference is a viable therapeutic strategy for chondrosarcoma. Mol Cancer Res 2017;15:1714–21.
29. Fons NR, Sundaram RK, Breuer GA, Peng S, McLean RL, Kalathil AN, et al. PPM1D mutations silence NAPRT gene expression and confer NAMPT inhibitor sensitivity in glioma. Nat Commun 2019;10:3790.
30. Watson M, Roulston A, Bélec L, Billot X, Marcellus R, Bédard D, et al. The small molecule GMX1778 is a potent inhibitor of NAD+ biosynthesis: strategy for enhanced therapy in nicotinic acid phosphoribosyltransferase 1-deficient tumors. Mol Cell Biol 2009;29:5872–88.
31. Tateishi K, Wakimoto H, Iafrate AJ, Tanaka S, Loebel F, Lelic N, et al. Extreme vulnerability of IDH1 mutant cancers to NAD+ depletion. Cancer Cell 2015;28:773–84.
32. Slemmons KK, Deel MD, Lin Y-T, Oristian KM, Kuprasertkul N, Genadry KC, et al. A method to culture human alveolar rhabdomyosarcoma cell lines as rhabdospheres demonstrates an enrichment in stemness and Notch signaling. Biol Open 2021;10:bio050211.
33. Walter D, Satheesha S, Albrecht P, Bornhauser BC, D'Alessandro V, Oesch SM, et al. CD133 positive embryonal rhabdomyosarcoma stem-like cell population is enriched in rhabdospheres. PLoS One 2011;6:e19506.
34. Hasmann M, Schemainda I. FK866, a highly specific noncompetitive inhibitor of nicotinamide phosphoribosyltransferase, represents a novel mechanism for induction of tumor cell apoptosis. Cancer Res 2003;63:7436–42.
35. Korotchkina L, Kazyulkin D, Komarov PG, Polinsky A, Andrianova EL, Joshi S, et al. OT-82, a novel anticancer drug candidate that targets the strong dependence of hematological malignancies on NAD biosynthesis. Leukemia 2020;34:1828–39.
36. Sun W, Chatterjee B, Shern JF, Patidar R, Song Y, Wang Y, et al. Relationship of DNA methylation to mutational changes and transcriptional organization in fusion-positive and fusion-negative rhabdomyosarcoma. Int J Cancer 2019;144:2707–17.
37. Maksimovic J, Gordon L, Oshlack A. SWAN: subset-quantile within array normalization for illumina infinium HumanMethylation450 BeadChips. Genome Biol 2012;13:R44.
38. Aryee MJ, Jaffe AE, Corrada-Bravo H, Ladd-Acosta C, Feinberg AP, Hansen KD, et al. Minfi: a flexible and comprehensive Bioconductor package for the analysis of Infinium DNA methylation microarrays. Bioinformatics 2014;30:1363–9.
39. Shern JF, Chen L, Chmielecki J, Wei JS, Patidar R, Rosenberg M, et al. Comprehensive genomic analysis of rhabdomyosarcoma reveals a landscape of alterations affecting a common genetic axis in fusion-positive and fusion-negative tumors. Cancer Discov 2014;4:216–31.
40. Brohl AS, Sindiri S, Wei JS, Milewski D, Chou H-C, Song YK, et al. Immunotranscriptomic profiling of extracranial pediatric solid malignancies. Cell Rep 2021;37:110047.
41. Li B, Dewey CN. RSEM: accurate transcript quantification from RNA-Seq data with or without a reference genome. BMC Bioinformatics 2011;12:323.
42. Dobin A, Davis CA, Schlesinger F, Drenkow J, Zaleski C, Jha S, et al. STAR: ultrafast universal RNA-seq aligner. Bioinformatics 2013;29:15–21.
43. Robinson MD, McCarthy DJ, Smyth GK. edgeR: a Bioconductor package for differential expression analysis of digital gene expression data. Bioinformatics 2010;26:139–40.

44. Hinson ARP, Jones R, Crose LES, Belyea BC, Barr FG, Linardic CM. Human rhabdomyosarcoma cell lines for rhabdomyosarcoma research: utility and pitfalls. Front Oncol 2013;3:183.
45. Subedi A, Liu Q, Ayyathan DM, Sharon D, Cathelin S, Hosseini M, et al. Nicotinamide phosphoribosyltransferase inhibitors selectively induce apoptosis of AML stem cells by disrupting lipid homeostasis. Cell Stem Cell 2021;28:1851–67.e8.
46. Shames DS, Elkins K, Walter K, Holcomb T, Du P, Mohl D, et al. Loss of NAPRT1 expression by tumor-specific promoter methylation provides a novel predictive biomarker for NAMPT inhibitors. Clin Cancer Res 2013;19:6912–23.
47. Duarte-Pereira S, Pereira-Castro I, Silva SS, Correia MG, Neto C, da Costa LT, et al. Extensive regulation of nicotinate phosphoribosyltransferase (NAPRT) expression in human tissues and tumors. Oncotarget 2016;7:1973–83.
48. O'Brien T, Oeh J, Xiao Y, Liang X, Vanderbilt A, Qin A, et al. Supplementation of nicotinic acid with NAMPT inhibitors results in loss of in vivo efficacy in NAPRT1-deficient tumor models. Neoplasia 2013;15:1314–29.
49. Zhao G, Green CF, Hui Y-H, Prieto L, Shepard R, Dong S, et al. Discovery of a highly selective NAMPT inhibitor that demonstrates robust efficacy and improved retinal toxicity with nicotinic acid coadministration. Mol Cancer Ther 2017;16:2677–88.
50. Nair AB, Jacob S. A simple practice guide for dose conversion between animals and human. J Basic Clin Pharm 2016;7:27–31.
51. Chowdhry S, Zanca C, Rajkumar U, Koga T, Diao Y, Raviram R, et al. NAD metabolic dependency in cancer is shaped by gene amplification and enhancer remodelling. Nature 2019;569:570–5.
52. Murata MM, Kong X, Moncada E, Chen Y, Imamura H, Wang P, et al. NAD+ consumption by PARP1 in response to DNA damage triggers metabolic shift critical for damaged cell survival. Mol Biol Cell 2019;30:2584–97.
53. Tateishi K, Higuchi F, Miller JJ, Koerner MVA, Lelic N, Shankar GM, et al. The alkylating chemotherapeutic temozolomide induces metabolic stress in IDH1-mutant cancers and potentiates NAD^+ depletion-mediated cytotoxicity. Cancer Res 2017;77:4102–15.
54. Redler J, Nelson AE, Heske CM. Mechanisms of resistance to NAMPT inhibitors in cancer. Cancer Drug Resist 2025;8:18.